ADVANCED ENGINEERING MATERIALS
www.aem-journal.com

Optical Printing of Conductive Silver on Ultrasmooth Nanocellulose Paper for Flexible Electronics

*Yueyue Pan, Zhen Qin, Sina Kheiri, Binbin Ying, Peng Pan, Ran Peng, and Xinyu Liu**

The nanofibrillated cellulose paper (nanocellulose paper or nanopaper), which is flexible, transparent, ultrasmooth, and biodegradable, has emerged as a new substrate material for the next generation of paper-based flexible electronics. Herein a visible light-induced printing technique for depositing highly conductive silver (Ag) patterns on nanopaper is reported. The optical Ag printing process is simple to implement at room temperature and only requires nontoxic, low-cost aqueous chemical solutions and an inexpensive light projection setup. The abundant carboxyl groups on the nanopaper enable efficient absorption of Ag^+ ions on the nanopaper surface for light-induced reduction of Ag^+ into a thin film of densely packed silver nanoparticles (AgNPs). Chemical annealing of the deposited AgNPs further enhances the conductivity of the printed Ag patterns. The mechanical and electrical properties of the printed Ag patterns on nanopaper are characterized, and the application of the optical Ag printing technique fabricating the nanopaper-based flexible circuits and electrochemical biosensors is also demonstrated. The optical printing technique will enable new designs and applications of nanopaper-based flexible electronics.

1. Introduction

Flexible electronics has been thriving for applications such as wearable devices, flexible displays, and bendable sensors because of its unique merits such as highly mechanical flexibility and stable electronic functionality under deformation, which cannot be achieved by traditional electronics.[1,2] In the past decades, significant research efforts have been spent on different aspects of flexible electronics, such as substrate/electronic materials, device designs, and large-scale integration. In terms of substrate materials, a variety of flexible substrates such as plastics, elastomers, textiles, and paper have been employed for constructing flexible electronic devices.[3–5]. Among these substrate materials, paper-based substrates are lightweight, biodegradable, less expensive, and environment friendly, and have been widely used in printed and flexible electronics and sensors.[6–8]

Nanofibrillated cellulose (NFC) paper (or simply "nanocellulose paper" or "nanopaper") is a new type of transparent paper substrate that benefits flexible electronics designs by virtue of its high transparency, ultrasmooth surface (with nanoscale roughness), high-density nanofiber matrix with nanoscale porosity, and physical/chemical compatibility with functional electronic materials.[9–16]

The plant-based nanocellulose is abundant on the planet and has a simple preparation process. Since the first fabrication of nanocellulose paper,[17] it has attracted great research interest on applying it to flexible electronics. The nanometer size of the nanocellulose fibers and their compact arrangement in the nanopaper dramatically reduce the light scattering in the nanopaper and thus endow it with high transparency, which has enabled the use of nanopaper in optoelectronics and energy applications.[12,18,19] The ultrasmooth surface, nanoscale porosity, and surface functional groups of the nanopaper make it an excellent substrate material for deposition and patterning of conductive and semiconductor materials.[16,20,21]

Several techniques have been used to deposit electronic materials onto paper substrates, including inkjet printing,[22,23] screen printing and spraying,[24,25] sputtering,[26,27] electron beam (E-beam) evaporation,[28] and optical printing.[29] By adjusting the physicochemical properties of inks, inkjet printing is competent for printing a multitude of conductive and semiconductor materials with micrometer-level resolution.[30] Screen printing and spraying[31,32] are simple processes, while there is a trade-off between the ease and resolution of the ink patterning. Sputtering and E-beam deposition[33] are combined with lithography-based patterning or shadow masking for high-resolution patterning of thin-film materials on flexible substrates, but these techniques require cleanroom facilities and thus are relatively expensive. Optical printing is a novel type of maskless printing technique with high resolution and relatively low cost. Apart

Y. Pan, Z. Qin, S. Kheiri, B. Ying, P. Pan, R. Peng, X. Liu
Department of Mechanical and Industrial Engineering
University of Toronto
5 King's College Road, Toronto, Ontario M5S 3G8, Canada
E-mail: xyliu@mie.utoronto.ca

B. Ying, P. Pan
Department of Mechanical Engineering
McGill University
817 Sherbrooke Street West, Montreal, QC H3A 0C3, Canada

R. Peng
Department of Marine Engineering
Dalian Maritime University
1 Lingshui Road, Dalian, Liaoning 116026, China

X. Liu
Institute of Biomedical Engineering
University of Toronto
164 College Street, Toronto, Ontario M5S 3G9, Canada

The ORCID identification number(s) for the author(s) of this article can be found under https://doi.org/10.1002/adem.202101598.

DOI: 10.1002/adem.202101598

from the laser-assisted methods based on optical trapping or laser-sintering,[34,35] a visible light-assisted optical printing technique was recently developed for photoreduction of metal ions in a room-temperature ink solution for high-quality metal deposition.[36] Silver (Ag) and palladium (Pd) micropatterns were printed, through a commercial projector, on a wide range of substrates such as silicon, glass, polymers, and office paper.

In this work, we extend this powerful optical printing technique to patterning highly conductive Ag on ultrasmooth nanopaper and fabricating nanopaper-based flexible electronics. With the abundant carboxyl groups on its surface, the 2,2,6,6-tetramethylpiperidine-1-oxyl radical (TEMPO)-oxidized nanopaper efficiently absorbs Ag^+ ions from a reductive chemical solution and thus allows reliable Ag deposition on its surface without additional treatment. The nanopaper-based flexible electronics benefit from the unique interface between the carboxyl functional groups and the deposited Ag nanoparticles (AgNPs), endowing the safe docking of the AgNPs and reliable adhesion of the printed Ag layer. We investigate the growth rate and conductivity of the silver layer on nanopaper and demonstrate the remarkable bendability with negligible conductivity change after up to 2000 times of folding/unfolding. The nanopaper-based circuits are resilient to 50 h water immersion and can tolerate high temperature up to 225 °C. We demonstrate the application of these Ag-printed nanopaper substrates to fabricating flexible electronics and biosensors. We believe that this optical Ag printing technique will enrich the fabrication tool set of nanopaper-based flexible sensors and electronics.

2. Results and Discussion

2.1. Nanopaper Characterization

The NFC-based nanopaper was fabricated through vacuum filtration, drying, and hot-pressing. The obtained nanopaper features high transparency (>90% in the visible range, Figure S1a,b, Supporting Information) and a flat ultrasmooth surface (roughness: 2.92 nm; Figure S1c, Supporting Information). The high transmittance (>80%; Figure S1b, Supporting Information) of nonprinted areas of the NFC paper can be maintained during the Ag printing. Thus, comparing to the 10–20% transmittance of the regular cellulose and nitrocellulose paper, our nanopaper substrate will provide a higher level of design flexibility for paper-based electronics that require transparent substrates.

2.2. Silver Printing on Nanopaper

The working principle of the optical Ag printing technique is based on visible light-assisted photoreduction of Ag^+ into AgNPs and chemical annealing-enabled sedimentation and interconnection of the deposited AgNPs. The "digital mask" defining the printing pattern was projected to the nanopaper substrate immerged in the $AgNO_3$ solution through a commercial projector. The schematic diagram and photograph of the experimental setup for Ag printing are shown in **Figure 1**a and Figure S2, Supporting Information, respectively. The Ag printing was achieved through the chemical reaction between $AgNO_3$ and Na_3Cit in the printing solution. The patterned light illumination from the projector enhances the electron transfer between Ag^+ and Cit^{3-}, thus facilitating the reduction of the Ag^+ into AgNPs. During the printing process, the Na_3Cit also serves as a capping agent to protect the seed Ag nuclei (Ag^0) from oxidation. The auxiliary $NaNO_3$ helps the flocculation of AgNPs on the nanopaper. The AgNPs deposited onto the nanopaper was chemically annealed by NaCl to further enhance the conductivity of the printed Ag patterns. The NaCl treatment helps remove the capped agent (Cit^{3-}) on the deposited AgNPs by introducing Cl^-, which enables more direct contact between AgNPs and thus further enhances the conductivity of the printed Ag patterns.

Comparing to other types of printed flexible electronics, nanopaper-based silver printing features a "green" synthetic method with natural abundant materials. The TEMPO-oxidized NFC has a high carboxylate level (1.4 mmol g^{-1}). The functional groups on the nanopaper surface could facilitate the formation of AgNPs in three different ways. First, the hydroxyl groups on nanopaper could anchor the metal nanoparticles through ion–dipole interaction.[39] Besides, the abundant carboxyl groups ($-COO^-$), as one of the unique features of TEMPO-oxidized NFC, increase the total amount of negative charges on the NFC surface, further boosting the absorption of the Ag^+ through electrostatic forces.[40] This unique merit makes the TEMPO-oxidized NFC stand out from other types of nanopaper which lack the negatively charged carboxyl groups. Moreover, the carboxyl groups are effective stabilization sites for AgNPs, providing the docking site to take over AgNPs from the reducing agent Na_3Cit in the Ag ink.[41–43]

A nanopaper-based printed circuit board (PCB) was fabricated using the optical printing technique, as shown in Figure 1b. The patterned Ag connections on the PCB cover an area of 7.5 mm × 5 mm. A series of Ag traces with different widths were printed on nanopaper (Figure 1c). One can see that 100 μm-wide Ag traces can be reliably printed with clear boundaries. The printing resolution can be further improved by using a projector with higher resolution. The nanopaper-based PCBs are sustainable and environmentally friendly. They can be easily disposed and recycled by incineration.[44] Figure 1d illustrates the incineration process of a nanopaper-based PCB. Owing to the ecofriendly constitution, it burnt out in 3 s and left only ashes of the inflammable silver with lightweight (Figure S3, Supporting Information).

2.3. Characterization of the Printed Silver

The printed Ag pattern was characterized with different techniques. **Figure 2**a shows the optical microscopic image of the Ag patterns on a nanopaper-based PCB. One can see that the edges of the printed Ag traces are clear and well-defined, and their widths are uniform. The energy-dispersive X-ray (EDX) spectroscopy images showing the oxygen and Ag element distributions in the same area are shown in Figure 2b,c, respectively. The nonprinted areas of the nanopaper have uniform oxygen element distribution, while the printed Ag traces show uniform Ag element distribution. Figure 2d illustrates the Ag intensity map of the cross-section of the printed pattern, showing a thin continuous layer of the printed Ag. The EDX and X-ray diffraction (XRD) spectra of the printed silver pattern, as shown in Figure 2e, further confirm the printed layer are primarily metallic Ag with

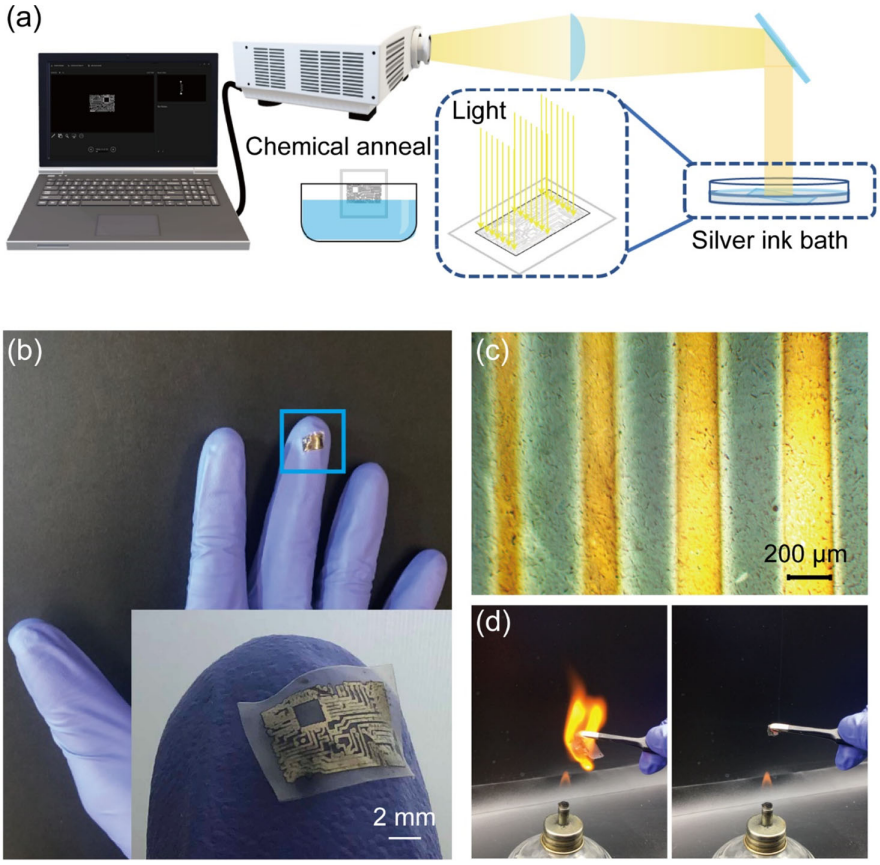

Figure 1. Visible light-assisted optical printing of highly conductive Ag patterns on nanopaper. a) The schematic of the printing setup. b) Ag circuit patterns printed on a piece of nanopaper. c) Four printed Ag connections with varied widths. d) The incineration process of a nanopaper-based printed circuit.

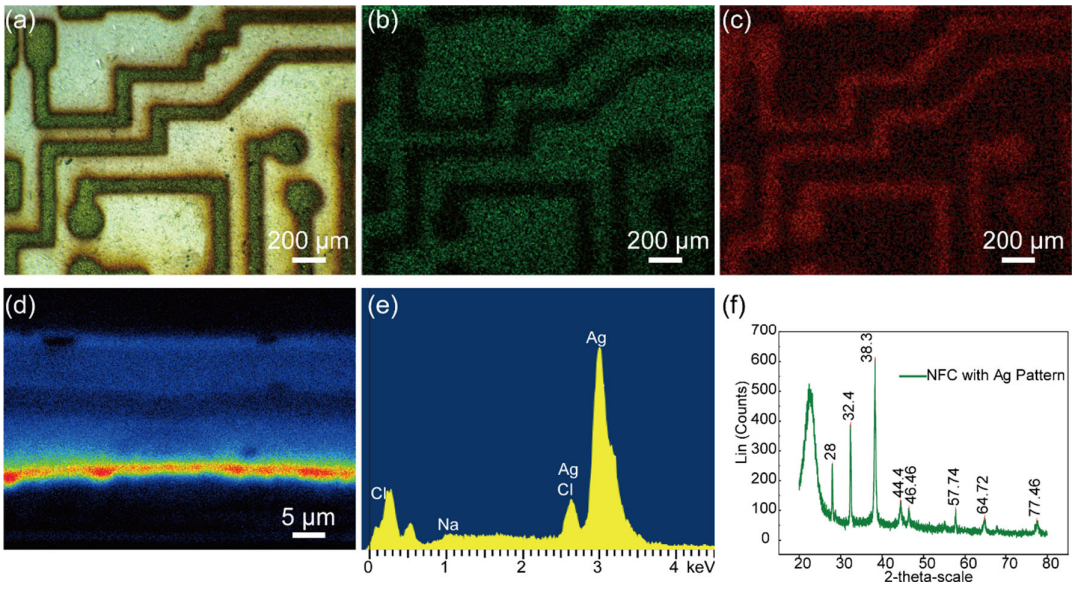

Figure 2. Characterization of the printed Ag patterns. a) The optical microscopic image of the printed Ag patterns on nanopaper. b,c) The elemental maps of (b) O (from the nanopaper substrate) and (c) Ag (from the printed patterns). d) The Ag intensity map of the sample cross-section. e) EDX spectra of the printed pattern on the nanopaper. f) XRD pattern of the sample.

minor AgCl and Ag_2O residuals.[45,46] The silver printed on the nanopaper was further characterized with scanning electron microscopy (SEM) (Figure S4, Supporting Information). One can see that the silver nanoparticles are compactly arranged and form a coalescent silver layer, verifying the high conductivity of the printed pattern. Regular cellulose paper usually consists of cellulose microfibers packed in a porous network, and its porous surface makes it hard to form a continuous and plat layer of densely packed AgNPs after NaCl annealing. As illustrated in the Figure S1, Supporting Information, the nanopaper has a nanoscale porosity, which supports the interconnection of the AgNPs and facilitates the metallization.

Cross-section of the silver patterned on nanopaper was also characterized with the EDX (Figure 2d and Figure S5, Supporting Information). The complementary intensity of the silver and carbon illustrates the distinct interface of the printed Ag and nanopaper. Although the nanoscale porosity facilitates the horizontally interlinking of Ag, it limits the vertical diffusion and infiltration of the Ag^+ and Ag^0 into the interior nanopaper. Thanks to the carboxyl and hydroxyl groups in the nanopaper which effectively attract silver ions from Ag ink, and the silver layer can well adhere to the nanopaper surface.

The optimization of the silver ink recipe has been investigated previously,[36] and we mainly focused on tuning the printing time. To explore the optimal Ag printing time for the nanopaper, we measured the thickness and resistance of printed Ag traces (0.79 mm wide and 5.5 mm long) as a function of the printing time. The conductivity was calculated based on the measured thickness/resistance and the Ag pattern width/length. From **Figure 3**a,b, one can see that the thickness of the printed Ag increases with the printing time. Various parameters have been investigated as the governing factors of nucleation and growth of the AgNP in the photochemical process, including the reaction temperature, pH, precursor, and so on.[47] One possible reason for the distinct stages of thickness gradient in our silver printing could be the weak yet gentle reductant citrate.[48] Based on the previously expatiated silver photoreduction and the growth property in our process, the growth of AgNP was analyzed as follows.[47,49,50] The thickness increase undergoes relatively slow stages (0–30 min, 30–50 min, and 70–80 min) and one rapid growth period (50–60 min). In the initial growth period (0–30 min), Ag^0 just starts to form and dot on the illumination region, while the overlying of AgNPs has not started and the conductivity is the lowest. With enough Ag^0 covering the surface of nanopaper, the horizontal fusion of AgNPs and larger Ag cluster formation starts at 30 min, resulting in the slow increase in thickness while dramatic increase in conductivity. The rapid increase of thickness at illumination within 50 to 60 min could be the explained by the unidirectional stacking of AgNPs as the gaps between the underlayer AgNPs have been filled in earlier reaction. It has been reported that the morphology and stacking of AgNP were variable, which was possibly caused by twinning in the presence of cellulose nanocrystals.[51] With illumination longer than 60 min, newly formed AgNPs start to fill the nanogaps between the AgNPs formed in the previous rapid growth stage, slowing down the increase in thickness again.

The conductivity of the Ag connection reaches saturation after 40 min printing, which can be attributed to the limited diffusion depth of the NaCl into a thick Ag layer (for chemical annealing). For a printing time of more than 40 min, the diffusion of the NaCl into the deeper AgNPs for annealing is harder to be achieved, therefore resulting in a decrease in conductivity when the printing time is longer than 40 min. It has been previously reported that chloride ions are most effective in chemical annealing to enhance the conductivity of silver film.[52] The enhancement was based on the self-catalytic addition of silver ions to the silver film, which increases the crystalline size of AgNP by Ostwald ripening. From the XRD pattern showed in Figure 2f, one can see that there is chloride element presented in the silver film, indicating there is silver chloride formed in the silver film at the same time. It is speculated that the silver chloride hinders the further diffusion of chloride ions into the deeper silver layer. Although longer illumination facilitates the formation of the thicker silver layer, the insufficient chemical anneal results in the decrease of conductivity.

The highest conductivity we achieved is 1.03×10^7 S m^{-1} with a printing time of 40 min (Ag thickness: 190 nm). Accordingly, we fixed the printing time at 40 min for all the subsequent experiments. The highest conductivity we achieved using our optical printing technique is comparable to that (2×10^7 S m^{-1}) of inkjet-printed Ag with a thickness of 3 μm[53] and is one order of magnitude higher than that (2.2×10^6 S m^{-1}) of a vacuum-filtered Ag-nanowire electrode (thickness: 300 nm).[54]

As reported in our previous work, nanopaper is expected to be a competent substrate in flexible electronics for its superior mechanical properties (Young's modulus: 10.02 GPa).[38] The foldability of the Ag-printed nanopaper was investigated through

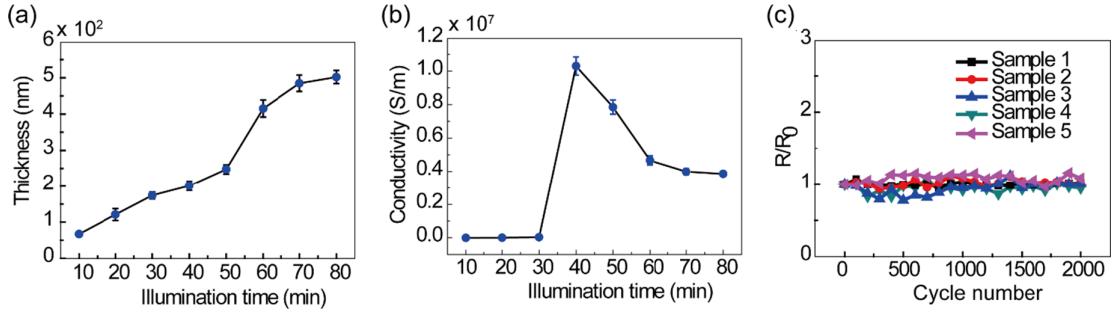

Figure 3. Characterization of the printed Ag pattern. a) The thickness of Ag layer versus the illumination time ($n = 5$). b) The conductivity of the Ag layer versus the illumination time ($n = 5$). c) The relative resistance changes of Ag patterns during 2000 cycles of repeated substrate folding and unfolding.

repeated folding and unfolding testing. Ag traces printed on nanopaper (width: 0.5 mm; length: 7.45 mm) were folded to 180° with a 1 mm folding radius and then unfolded to its original flat status, and this folding/unfolding process was repeated for 2000 cycles. During the folding/unfolding process, the resistance of each electrode remained at a relatively stable level without significant decrease (Figure 3c), showing excellent mechanical stability of the printed Ag on nanopaper. The water stability of the printed Ag was also explored. We immersed Ag traces of 0.78 mm wide and 11.4 mm long in DI water for 10 h, dried them at 20 °C for 10 h, and then measured the resistance of each electrode. As shown in Figure S6, Supporting Information, the electrode resistance remained stable after five cycles of water immersion and drying. Investigation on the thermal stability was measured on a printed three-electrode-cell silver pattern on the nanopaper. The silver pattern was baked on a hot plate at 50, 100, 150, 200, and 225 °C sequentially (1 min at each temperature), and an infrared thermometer was used to confirm the temperature on the silver electrode surface. After baking, the silver pattern was taken down to recover back to room temperature. The resistance of working electrode was measured with a multimeter and the value maintained stable in the range of 25 to 225 °C, as illustrated in Figure S7a,b, Supporting Information. It should be noted that there was a recoverable deformation on nanopaper in the range of 100 to 200 °C. While at 225 °C, an irreversible swell and fatigue occurred to the nanopaper. The nanopaper was also severely oxidized and lost the high transmittance.

The thermal stability of the nanopaper substrate and the nanopaper patterned with silver was also characterized via thermogravimetric analysis (TGA) using a simultaneous thermal analyzer. Approximately 20 mg of the Ag-patterned nanopaper was heated from 20 to 600 °C at a heating rate of 10 °C min^{-1} in an N_2 atmosphere. Figure S7c, Supporting Information, shows the TGA and derivative thermogravimetry (DTG) curves of the nanopaper-based silver circuit. Initial weight loss at temperature lower than 100 °C is attributed to the moisture release of nanopaper. The weight loss at the stage 200 to 360 °C refers to the decomposition of cellulose, and the final stage (360 to 600 °C) of weight loss indicates the decomposition to ash. The nanopaper-based silver circuit possesses a comparable thermal resistance to the commonly used PCB.[55] Based on the thermal analysis and the conductivity stability, one could see that the nanopaper-based silver pattern possesses a good thermal stability in the range of 25 to 200 °C. The thermal stability of the nanopaper and the silver circuit on nanopaper is consistent with that of NFC-based electronics reported previously.[15]

The above characterization results demonstrate that the printed Ag patterns on nanopaper are uniform, precise, and highly conductive. The cyclic folding/unfolding and wetting–drying tests also prove that the nanopaper-based Ag patterns are stable mechanically and electrically. We believe that our optical Ag printing technique is suitable for fabricating nanopaper-based flexible electronics with good mechanical and electrical stability.

2.4. Demonstrations for Flexible Electronics and Biosensors

To demonstrate the application of the optical Ag printing technique, we fabricated several nanopaper-based functional circuits with surface-mount electrical components. For fabricating each circuit, a piece of nanopaper was first printed with Ag trace connections to form a PCB, and surface mount components, such as resistors, capacitors, light-emitting diodes (LED), and operational amplifiers (op-amps), were then attached to the PCB at their corresponding mounting positions using superglue and electrically connected to the Ag connections with Ag ink (E2414, Ercon). **Figure 4**a shows a maple-leaf-shaped circuit with an LED, and two flat alligator clips were used to apply 3 V to light up the LED. We also built a paper house with transparent nanopaper windows, and LED circuits were printed on inside surfaces of the nanopaper windows for lighting (Figure 4b). From the zoomed view of Figure 4b, one can see that the LED circuits on the left and right nanopaper windows were printed along the vertical and horizontal directions, respectively, and thus bended along these two orthogonal directions once the cylindrical house wall was formed. The LED circuits still remain functional under these bending modes, showing the mechanical robustness of the nanopaper-based flexible circuit.

We also fabricated nanopaper-based op-amp circuits for signal conditioning. Figure 4c shows a non-inverting op-amp circuit built on nanopaper with a closed-loop gain of 101. The measured input–output voltage relationship of the circuit is plotted in Figure 4d, which has a saturation voltage of 2.4 V. Similarly, a first-order low-pass filter circuit (Figure 4e) was built with an op-amp, a capacitor, and three resistors. A 1 Hz sinusoidal signal coupled with a 14 Hz sinusoidal noise can be successfully denoized, as shown in Figure 4f. The circuit diagrams of the two op-amp circuits (Figure 4c,e) are shown in Figure S8, Supporting Information. These op-amp circuits demonstrate that the optically printed Ag circuits can work with both direct-current (DC) and alternating-current (AC) signals. Note that the layout of our nanopaper-based circuit could be more compact than that of other paper-based circuits[56,57] because of the high resolution of Ag printing.

Finally, we applied the optical Ag printing technique to fabrication of nanopaper-based electrochemical biosensors. Paper-based analytical devices have been widely used for low-cost disease diagnostics,[58–61] environmental monitoring,[62,63] and food testing.[64,65] Nanopaper-based devices have also been developed for optical chemical sensing[37] and biosensing.[38] As a proof-of-concept demonstration, we printed a working electrodes (WE), a counter electrode (CE), and a reference electrode (RE) on nanopaper through Ag printing to form a three-electrode electrochemical cell (**Figure 5**a). The electrochemical biosensor was experimentally characterized through cyclic voltammetry (CV) using 10 mM $K_3[Fe(CN)_6]$ in 1 M KCl as a model electroactive compound. In the experiments, 10 µL of $K_3[Fe(CN)_6]$ was first added to cover the three electrodes, and CV curves were captured at different scan rates. As shown in Figure 5b, the measured CV curves reveal a typical reversible (Nernstian) electrochemical reaction.[66]

Glucose detection was demonstrated using the nanopaper-based electrochemical biosensor, and the detailed protocol can be found in our previous work.[67] Chronoamperometry (CA) was performed on the biosensor for glucose detection. The principle of glucose detection is based on the quantification of

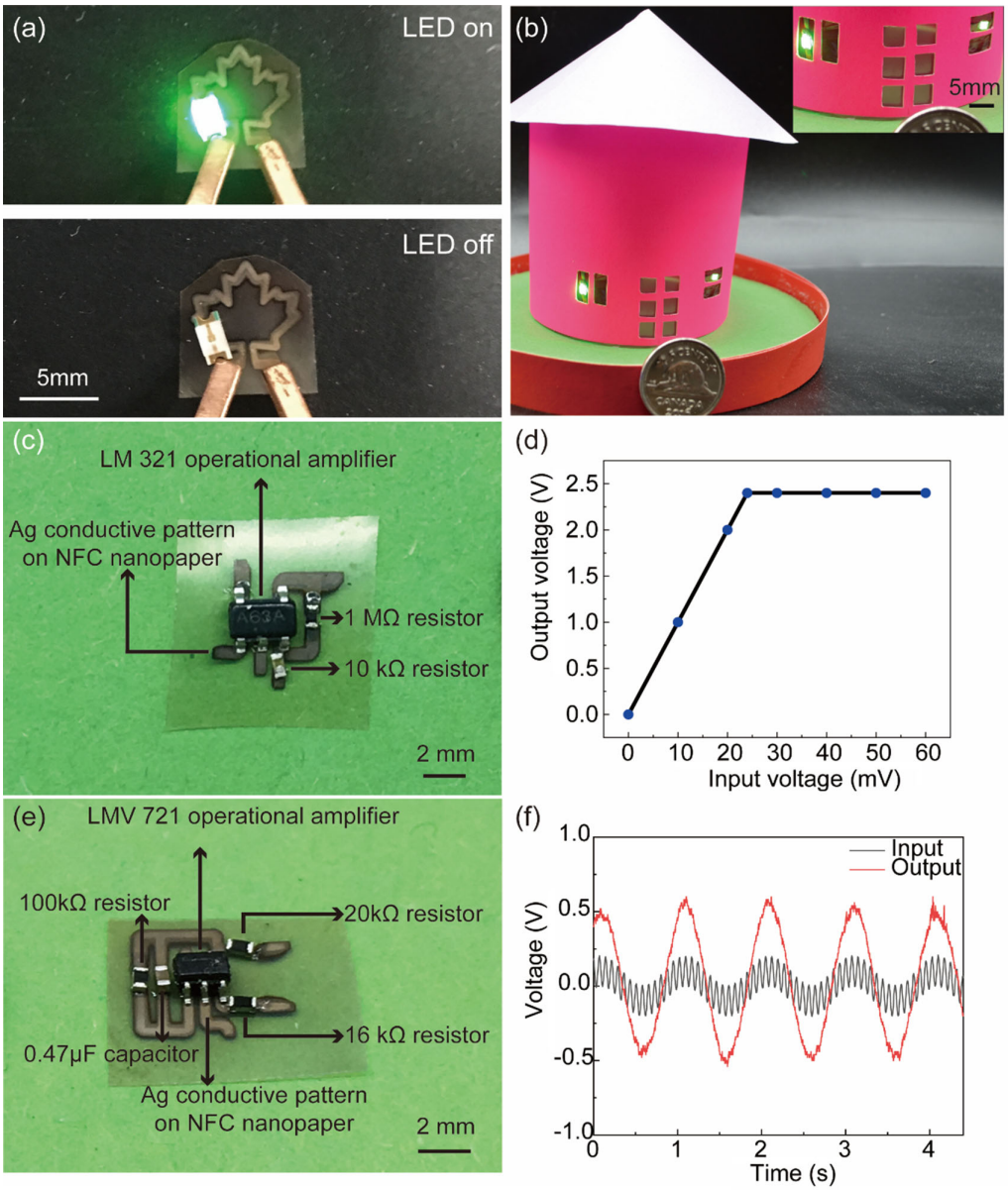

Figure 4. Nanopaper-based flexible circuits. a) A maple-leaf-shaped LED circuit printed on nanopaper. b) A paper house with transparent nanopaper windows and LED lights on the windows. c) A non-inverting op-amp circuit built on nanopaper. d) The input–output voltage relationship of the non-inverting circuit in (c). e) A first-order low-pass filter circuit built on nanopaper. f) The input/output signals of the low-pass filter.

$Fe(CN)_6^{4-}$ obtained in the process of glucose oxidase (GO_x)-catalyzed oxidation of glucose, which can be quantified from the measured CA currents. In brief, 2 μL of GO_x (2.5 mg mL^{-1} in 10 mM $K_3[Fe(CN)_6]$ and 1 M KCl) was added onto the WE and incubated for 5 min. 5 μL of glucose-spiked PBS at different concentrations (0–20 mM) was then added to the reaction zone to cover the three electrodes. After 1 min incubation, a 0.5 V step potential was applied to the WE (versus the RE), and the resultant CA current was recorded. The average current value during 119–120 s was calculated as the sensor readout. Figure 5c illustrates the measured CA currents at different glucose concentrations, and Figure 5d shows the calibration curve of the glucose biosensor. The limit of detection (LOD) is the glucose biosensor was determined to be 0.84 mM, which is comparable to existing paper-based glucose sensors.[67–69]

Note that, for fabricating electrochemical sensors, the pure Ag electrode surface has the oxidation issue that affects the device's performance stability.[70,71] Apart from Ag, other more stable metal materials such as platinum and gold can be printed using the same optical printing technique.[72–74] An additional layer of

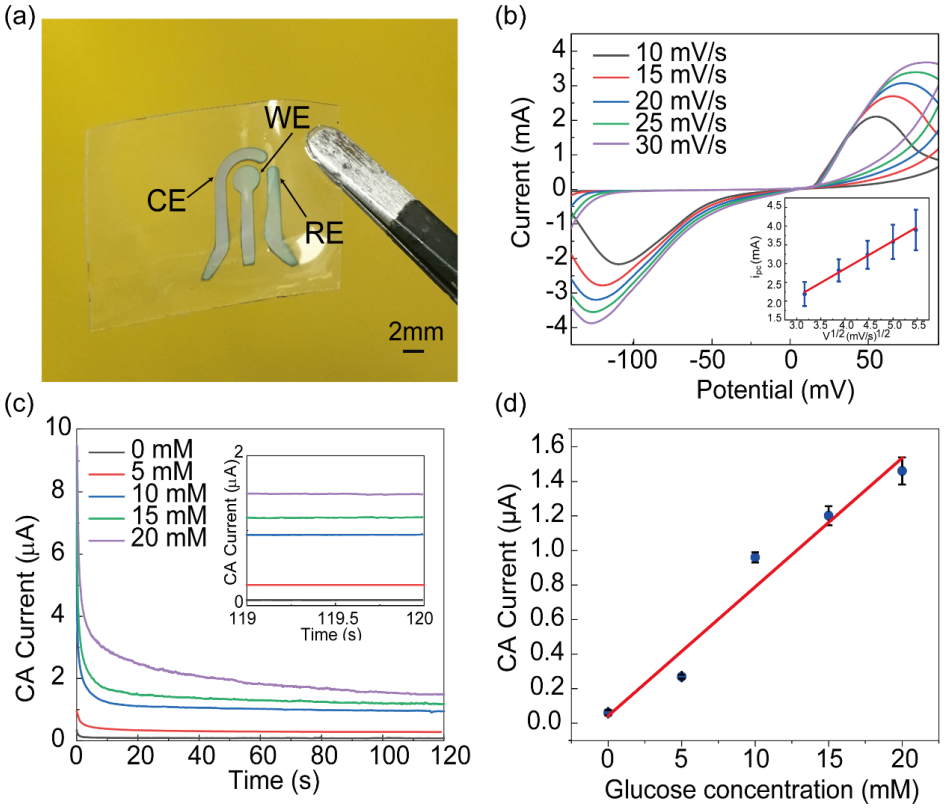

Figure 5. Nanopaper-based electrochemical biosensor for glucose detection. a) Photograph of the three printed Ag electrodes on nanopaper. b) CV characterization of the biosensor at varied scanning rates. Insets: Data plot of the anodic peak current versus square root of the scan rate, where the solid line is a linear fit with the regression equation: $y = 0.741x - 0.103$, ($R^2 = 0.99$, $n = 5$). c) Typical CA current plots at different glucose concentrations. d) The calibration plot of the glucose sensor. The solid line represents a linear fit with the regression equation: $y = 0.075x + 0.043$ ($R^2 = 0.96$, $n = 4$).

more stable platinum or gold can be deposited onto the Ag electrodes to minimize the electrode surface oxidation and improve the device stability.

3. Conclusion

This paper reported the visible light-assisted optical Ag printing technique for fabricating flexible electronics on transparent nanopaper. The technique is rapid, ecofriendly, and low-cost and provides micrometer resolution. The Ag pattern on nanopaper is highly conductive, foldable, and mechanically and electrically stable. We demonstrated the versatility of our technique for fabricating nanopaper-based flexible circuits and biosensors. Simple LED circuits, functional op-amp circuits were successfully constructed and tested. We also fabricated a nanopaper-based electrochemical biosensor and applied it to glucose detection. The optical printing technique holds great potential in the fields of nanopaper-based flexible (opto)electronics and biosensing.

4. Experimental Section

Reagents and Materials: TEMPO-oxidized NFC slurry (catalog number: CNF-1; 1.0 wt% solid, carboxylate level 1.4 mmol g^{-1} solid, and average nanofiber diameter: 10 nm) was purchased from the Process Development Center at the University of Maine (Orono, ME). Durapore hydrophobic polyvinyl difluoride (PVDF) membrane filters with a 0.45 μm pore size (catalog number: HVLP09050) was purchased from Millipore Canada (Etobicoke, ON). Sodium nitrate ($NaNO_3$, >99%) was purchased from Bio Basic Canada (Markham, ON). Potassium ferrocyanide ($K_4[Fe(CN)_6]\cdot 3H_2O$], ACS grade), silver nitrate ($AgNO_3$, ACS grade), and sodium chloride (NaCl, >99.0%) were purchased from BioShop Canada (Burlington, ON). Phosphate-buffered saline (PBS) was purchased from Gibco, NY, USA. D-(+)-glucose, glucose oxidase (from Aspergillus niger, 147.9 U mg^{-1}), and sodium citrate dihydrate ($Na_3C_6H_5O_7\cdot 2H_2O$, 99.0%) were purchased from Sigma Aldrich Canada (Oakville, ON). All chemicals and reagents were used as received without further purification. Deionized (DI) water was used in preparing all chemical solutions.

Nanopaper Fabrication: The NFC-based nanopaper was prepared using a modified vacuum filtration method.[37,38] The NFC gel dispersion was prepared by adding 20 g of NFC slurry in DI water for a final concentration of 1 wt%. The solution was thoroughly mixed via stirring at 1100 rpm for 2 h. The dispersion was then poured to a filtration chamber (BP-1755 Filterware 90 mm microfiltration glassware, Wilmad-Labglass) and vacuum-filtered using the 0.45 μm pore membrane for 20 h. The filtration process eventually formed a dry layer of nanopaper on top of the filter paper. After that, the nanopaper was sandwiched between two pairs of Teflon sheets (from bottom to top: 0.039" thick Teflon, 0.002" thick Teflon film, nanopaper, 0.002" thick Teflon film, and 0.039" thick Teflon) and hot-pressed on a 12-ton hydraulic laboratory press (Carver, Inc., Model #3912) under 2.6 MPa at 85 °C for 10 min to form a flat nanopaper. A fabricated nanopaper is highly transparent with an ultrasmooth surface, as characterized in Figure S1, Supporting Information.

Preparation of the Chemical Solution for Ag Printing: The chemical solution for Ag printing was prepared according to a previously reported protocol.[36] Three chemicals, $NaNO_3$, $AgNO_3$, and Na_3Cit, were sequentially added to DI water to reach final concentrations of 150, 10, and 15 mM, respectively. Magnetic stirring was used to fully dissolve each chemical after addition.

Silver Printing Procedure: The silver patterns were printed through visible light-assisted reduction of Ag^+. The nanopaper was placed in a 35 mm Petri dish filled with 5 mL of the printing solution. The desired pattern was predesigned in AutoCAD as a "digital mask"' and played in a PowerPoint slide to project the visible light pattern onto the nanopaper via a 1080p commercial projector (BenQ MH530FHD; 3300 Lumens). The printing time ranged from 10 to 80 min. After printing, the sample was sequentially rinsed with DI water, 20 mM NaCl solution, and DI water again for chemical annealing of the deposited Ag nanoparticles (AgNPs). Finally, the sample was dried with a nitrogen gun. The Ag printing mechanism were discussed in the Results and Discussion section.

Characterization Methods: The transmittance of the nanopaper was measured with a UV/Vis spectrometer (Lambda 1050). The surface morphology of the nanopaper was characterized by an atomic force microscope (AFM; Hitachi 5100N). The photographs of the printed Ag patterns were captured using a compound microscope (Motic, BA310) with a CMOS camera (Optixcam, Summit K2). Element analysis of the printed Ag circuits was performed using a scanning electron microscope (SEM; JEOL, 6610LV) equipped with an EDX spectrometer (Oxford Instruments, 20 mm^2 detector window, Peltier cooled silicon drift detector, and the INCA software provided by the vendor). The structural state and the phase identification in the printed pattern on nanopaper were measured with an XRD system (including the PW 1830 HT generator, PW 1050 goniometer, PW3710 control electronics, and the X-Pert system software). The resistance of the printed Ag connections on nanopaper was measured by a source meter (Keithley 6202) and a multimeter (B&K Precision, 2708B). The thickness of the Ag layer was measured by a profilometer (Dektak, AlphaStep 200). The thermal stability was measured by a simultaneous thermal analyzer (NETZSCH STA 449 F3 Jupiter). The printed operational amplifier (op-amp) circuits were tested using a functional generator (Keysight 33500B) and an oscilloscope (Tektronix TDS 2024C). The nanopaper-based electrochemical biosensor was characterized using a precision potentiostat (Autolab PGSTAT302N, Metrohm).

Supporting Information

Supporting Information is available from the Wiley Online Library or from the author.

Acknowledgements

The authors acknowledge the financial support from the Natural Sciences and Engineering Research Council of Canada (grant numbers: RGPIN-2017-06374, RGPAS-2017-507980, and DGDND-2017-00001), the Canada Foundation for Innovation (grant number: JELF-38428), and the University of Toronto (through the Percy Edward Hart Professorship to Xinyu Liu).

Conflict of Interest

The authors declare no conflict of interest.

Data Availability Statement

The data that support the findings of this study are available in the supplementary material of this article.

Keywords

conductive silver printing, electrochemical biosensors, flexible electronics, nanofibrillated cellulose paper, photoreduction

Received: November 22, 2021
Published online: January 14, 2022

[1] B. D. Gates, *Science* **2009**, *323*, 1566.
[2] A. Nathan, A. Ahnood, M. T. Cole, S. Lee, Y. Suzuki, P. Hiralal, F. Bonaccorso, T. Hasan, L. Garcia-Gancedo, A. Dyadyusha, S. Haque, P. Andrew, S. Hofmann, J. Moultrie, D. Chu, A. J. Flewitt, A. C. Ferrari, M. J. Kelly, J. Robertson, G. A. J. Amaratunga, W. I. Milne, *Proc. IEEE* **2012**, *100*, 1486.
[3] W. Gao, H. Ota, D. Kiriya, K. Takei, A. Javey, *Acc. Chem. Res.* **2019**, *52*, 523.
[4] P. Wang, M. Hu, H. Wang, Z. Chen, Y. Feng, J. Wang, W. Ling, Y. Huang, *Adv. Sci.* **2020**, *7*, 1.
[5] G. Chen, Y. Li, M. Bick, J. Chen, *Chem. Rev.* **2020**, *120*, 3668.
[6] P. Song, Y. H. Wang, X. Liu, *Flex. Print. Electron.* **2017**, *2*, 034001.
[7] Y. H. Wang, P. Song, X. Li, C. Ru, G. Ferrari, P. Balasubramanian, M. Amabili, Y. Sun, X. Liu, *Micromachines* **2018**, *9*, 19.
[8] D. Ha, Z. Fang, N. B. Zhitenev, *Adv. Electron. Mater.* **2018**, *4*, 1.
[9] Y. Zhang, L. Zhang, K. Cui, S. Ge, X. Cheng, M. Yan, J. Yu, H. Liu, *Adv. Mater.* **2018**, *30*, 1.
[10] X. Xu, F. Liu, L. Jiang, J. Y. Zhu, D. Haagenson, D. P. Wiesenborn, *ACS Appl. Mater. Interfaces* **2013**, *5*, 2999.
[11] H. Sehaqui, Q. Zhou, O. Ikkala, L. A. Berglund, *Biomacromolecules* **2011**, *12*, 3638.
[12] Z. Fang, H. Zhu, Y. Yuan, D. Ha, S. Zhu, C. Preston, Q. Chen, Y. Li, X. Han, S. Lee, G. Chen, T. Li, J. Munday, J. Huang, L. Hu, *Nano Lett.* **2014**, *14*, 765.
[13] J. Huang, H. Zhu, Y. Chen, C. Preston, K. Rohrbach, J. Cumings, L. Hu, *ACS Nano* **2013**, *7*, 2106.
[14] E. Lizundia, M. Delgado-Aguilar, P. Mutjé, E. Fernández, B. Robles-Hernandez, M. R. de la Fuente, J. L. Vilas, L. M. León, *Cellulose* **2016**, *23*, 1997.
[15] Y. H. Jung, T. H. Chang, H. Zhang, C. Yao, Q. Zheng, V. W. Yang, H. Mi, M. Kim, S. J. Cho, D. W. Park, H. Jiang, J. Lee, Y. Qiu, W. Zhou, Z. Cai, S. Gong, Z. Ma, *Nat. Commun.* **2015**, *6*, 1.
[16] F. Hoeng, A. Denneulin, J. Bras, *Nanoscale* **2016**, *8*, 13131.
[17] M. Nogi, S. Iwamoto, A. N. Nakagaito, H. Yano, *Adv. Mater.* **2009**, *21*, 1595.
[18] L. Hu, G. Zheng, J. Yao, N. Liu, B. Weil, M. Eskilsson, E. Karabulut, Z. Ruan, S. Fan, J. T. Bloking, M. D. McGehee, L. Wågberg, Y. Cui, *Energy Environ. Sci.* **2013**, *6*, 513.
[19] O. A. T. Dias, S. Konar, A. L. Leão, W. Yang, J. Tjong, M. Sain, *Front. Chem.* **2020**, *8*, 420.
[20] J. M. Malho, P. Laaksonen, A. Walther, O. Ikkala, M. B. Linder, *Biomacromolecules* **2012**, *13*, 1093.
[21] G. Zheng, Y. Cui, E. Karabulut, L. Wågberg, H. Zhu, L. Hu, *MRS Bull.* **2013**, *38*, 320.
[22] K. Yamada, T. G. Henares, K. Suzuki, D. Citterio, *Angew. Chem. Int. Ed.* **2015**, *54*, 5294.
[23] N. C. Raut, K. Al-Shamery, *J. Mater. Chem. C* **2018**, *6*, 1618.
[24] W. J. Hyun, E. B. Secor, M. C. Hersam, C. D. Frisbie, L. F. Francis, *Adv. Mater.* **2015**, *27*, 109.
[25] L. Wang, J. Liu, *ECS J. Solid State Sci. Technol.* **2015**, *4*, P3057.
[26] L. Gomes, A. Marques, A. Branco, J. Araújo, M. Simões, S. Cardoso, F. Silva, I. Henriques, C. A. T. Laia, C. Costa, *Displays* **2013**, *34*, 326.

[27] D. M. Mihut, A. Afshar, L. W. Lackey, K. N. Le, *Surf. Coatings Technol.* **2019**, *368*, 59.
[28] P. Peinado, S. Sangiao, J. M. De Teresa, *ACS Nano* **2015**, *9*, 6139.
[29] A. S. Urban, A. A. Lutich, F. D. Stefani, J. Feldmann, *Nano Lett.* **2010**, *10*, 4794.
[30] M. Singh, H. M. Haverinen, P. Dhagat, G. E. Jabbour, *Adv. Mater.* **2010**, *22*, 673.
[31] P. J. Lamas-Ardisana, P. Casuso, I. Fernandez-Gauna, G. Martínez-Paredes, E. Jubete, L. Añorga, G. Cabañero, H. J. Grande, *Electrochem. Commun.* **2017**, *75*, 25.
[32] S. Thiemann, S. J. Sachnov, F. Pettersson, R. Bollström, R. Österbacka, P. Wasserscheid, J. Zaumseil, *Adv. Funct. Mater.* **2014**, *24*, 625.
[33] M. C. Hsieh, C. Kim, M. Nogi, K. Suganuma, *Nanoscale* **2013**, *5*, 9289.
[34] Y. Bao, Z. Yan, N. F. Scherer, *J. Phys. Chem. C* **2014**, *118*, 19315.
[35] S. Liu, M. C. Yuen, R. Kramer-Bottiglio, *Flex. Print. Electron.* **2019**, *4*, 015004.
[36] X. Yang, M. Sun, Y. Bian, X. He, *Adv. Funct. Mater.* **2019**, *29*, 1807615.
[37] L. Chen, B. Ying, P. Song, X. Liu, *Adv. Mater. Interfaces* **2019**, *6*, 1901346.
[38] B. Ying, S. Park, L. Chen, X. Dong, E. W. K. Young, X. Liu, *Lab Chip* **2020**, *20*, 3322.
[39] J. He, T. Kunitake, A. Nakao, *Chem. Mater.* **2003**, *15*, 4401.
[40] F. Jiang, Y. Lo Hsieh, *Biomacromolecules* **2014**, *15*, 3608.
[41] O. Sambalova, K. Thorwarth, N. V. Heeb, D. Bleiner, Y. Zhang, A. Borgschulte, A. Kroll, *ACS Omega* **2017**, *3*, 724.
[42] T. Saito, A. Isogai, *Carbohydr. Polym.* **2005**, *61*, 183.
[43] J. Song, N. L. Birbach, J. P. Hinestroza, *Cellulose* **2012**, *19*, 411.
[44] Y. Zhou, C. Fuentes-Hernandez, T. M. Khan, J. C. Liu, J. Hsu, J. W. Shim, A. Dindar, J. P. Youngblood, R. J. Moon, B. Kippelen, *Sci. Rep.* **2013**, *3*, 24.
[45] M. S. Al Aboody, *Artif. Cells, Nanomed. Biotechnol.* **2019**, *47*, 2107.
[46] W. Zhou, H. Liu, J. Wang, D. Liu, G. Du, J. Cui, *ACS Appl. Mater. Interfaces* **2010**, *2*, 2385.
[47] S. H. Lee, B. H. Jun, *Int. J. Mol. Sci.* **2019**, *20*, 2651.
[48] X. Dong, X. Ji, H. Wu, L. Zhao, J. Li, W. Yang, *J. Phys. Chem. C* **2009**, *113*, 6573.
[49] N. T. K. Thanh, N. Maclean, S. Mahiddine, *Chem. Rev.* **2014**, *114*, 7610.
[50] M. Harada, E. Katagiri, *Langmuir* **2010**, *26*, 17896.
[51] Z. Hosseinidoust, M. Basnet, T. G. M. Van De Ven, N. Tufenkji, *Environ. Sci. Nano* **2016**, *3*, 1259.
[52] D. Y. Shin, G. R. Yi, D. Lee, J. Park, Y. B. Lee, I. Hwang, S. Chun, *Nanoscale* **2013**, *5*, 5043.
[53] H. Saghlatoon, L. Sydanheimo, L. Ukkonen, M. Tentzeris, *IEEE Antennas Wirel. Propag. Lett.* **2014**, *13*, 915.
[54] M. Yang, S. W. Kim, S. Zhang, D. Y. Park, C. W. Lee, Y. H. Ko, H. Yang, Y. Xiao, G. Chen, M. Li, *J. Mater. Chem. C* **2018**, *6*, 7207.
[55] P. Evangelopoulos, E. Kantarelis, W. Yang, *J. Anal. Appl. Pyrolysis* **2015**, *115*, 337.
[56] M. M. Hamedi, A. Ainla, F. Güder, D. C. Christodouleas, M. T. Fernández-Abedul, G. M. Whitesides, *Adv. Mater.* **2016**, *28*, 5054.
[57] K. Kim, H. Jang, C. W. Park, H. K. Park, S. Choi, *ICCAS 2015-2015 15th Int. Conf. Control. Autom. Syst. Proc.*, Busan, Korea (South) **2015**, p. 1857.
[58] X. Li, Z. Qin, H. Fu, T. Li, R. Peng, Z. Li, J. M. Rini, X. Liu, *Biosens. Bioelectron.* **2021**, *177*, 112672.
[59] X. Li, X. Liu, *Adv. Healthc. Mater.* **2016**, *5*, 1326.
[60] T. Ozer, C. McMahon, C. S. Henry, *Annu. Rev. Anal. Chem.* **2020**, *13*, 85.
[61] R. P. S. De Campos, D. G. Rackus, R. Shih, C. Zhao, X. Liu, A. R. Wheeler, *Anal. Chem.* **2019**, *91*, 2506.
[62] N. A. Meredith, C. Quinn, D. M. Cate, T. H. Reilly, J. Volckens, C. S. Henry, *Analyst* **2016**, *141*, 1874.
[63] C. Zhao, L. Chen, G. Zhong, Q. Wu, J. Liu, X. Liu, *Water Res.* **2021**, *202*, 117410.
[64] Y. Zhang, P. Zuo, B. C. Ye, *Biosens. Bioelectron.* **2015**, *68*, 14.
[65] E. Trofimchuk, Y. Hu, A. Nilghaz, M. Z. Hua, S. Sun, X. Lu, *Food Chem.* **2020**, *316*, 126396.
[66] A. J. Bard, L. R. Faulkner, *Electrochemical Methods Fundamentals and Applications*, Wiley, New York **2000**.
[67] C. Zhao, M. M. Thuo, X. Liu, *Sci. Technol. Adv. Mater.* **2013**, *14*, 54402.
[68] W. Dungchai, O. Chailapakul, C. S. Henry, *Anal. Chem.* **2009**, *81*, 5821.
[69] Z. Nie, F. Deiss, X. Liu, O. Akbulut, G. M. Whitesides, *Lab Chip* **2010**, *10*, 3163.
[70] H. Sasaki, S. Toshima, *Electrochim. Acta* **1975**, *20*, 201.
[71] A. Bayesov, E. Tuleshova, A. Tukibayeva, G. Aibolova, F. Baineyeva, *Orient. J. Chem.* **2015**, *31*, 1867.
[72] Y. Zhang, Z. Liang, A. P. Zhang, H. Y. Tam, *Adv. Opt. Mater.* **2021**, *9*, 1.
[73] M. M. Momeni, Y. Ghayeb, *J. Mater. Sci. Mater. Electron.* **2016**, *27*, 1062.
[74] Z. Zhao, J. Bai, Y. Yao, C. Wang, *Mater. Today* **2020**, *37*, 10.